Atmospheric Pollution Research 6 (2015) 322-333

Atmospheric Pollution Research

www.atmospolres.com

Impact of spatial resolution on air quality simulation: A case study in a highly industrialized area in Shanghai, China

Jiani Tan [1], Yan Zhang [1, 2], Weicun Ma [1], Qi Yu [1], Jian Wang [1], Limin Chen [1]

[1] *Shanghai Key Laboratory of Atmospheric Particle Pollution and Prevention (LAP3), Department of Environmental Science and Engineering, Fudan University, Shanghai 200433, PR China*

[2] *Jiangsu Key Laboratory of Atmospheric Environment Monitoring and Pollution Control (AEMPC), School of Environmental Sciences and Engineering, Nanjing University of Information Science and Technology, PR China*

ABSTRACT

The air pollution contribution from highly industrialized areas has been a prominent issue in regional air quality control. Particular emphasis on local industrial emissions is necessary to understand the complexity of air pollution over highly industrialized areas. Baoshan District, one of the most important industrialized areas in China and the most competitive steel and iron production base worldwide, was selected as the study area in this work. The WRF/CMAQ modeling system with local emission profile was applied to study the impact of spatial resolution on air quality modeling. The simulation results for SO_2, NO, NO_2, CO and PM_{10} at both 3–km and 1–km resolutions were verified by ground level observations. The results showed that the allocation of the emission inventory is improved by using finer resolution grids, which allow the consideration of detailed emission features. The influence of model resolution was more significant for air quality than for meteorology simulation. The relative errors using the finer resolution method ranged from –25% to 59%, an obvious improvement over the error value of 26%–245% obtained using the coarse resolution method. The changing tendencies of air pollutants in urban and rural areas were generally better modeled at finer than coarser resolution. However, the detailed variation in the most heavily polluted areas was still difficult to capture, and the model performance was not evidently improved by the use of a fine resolution. To improve the model performance over highly industrialized areas for future studies, combining the dynamic emission profile with detailed industrial activities and accurate local meteorological fields is suggested.

Keywords: *WRF/CMAQ, model evaluation, emission inventory, industrialized area, fine resolution*

Corresponding Author:
Yan Zhang
☎ : *+86-21-65642530*
🖷 : *+86-21-65642597*
✉ : *yan_zhang@fudan.edu.cn*

Article History:
Received: 03 July 2014
Revised: 10 October 2014
Accepted: 11 October 2014

doi: 10.5094/APR.2015.036

1. Introduction

Beginning in 2002, heavy industry has led a boom in the new, revived Chinese economy. However, the number of air pollution episodes has increased simultaneously, mainly in China's mega cities (Chan and Yao, 2008). Highly industrialized areas play very important roles in regional air pollution control. In some previous studies, the pollution status in highly industrialized areas (Tsai et al., 2007; Figueiredo et al., 2013; Tan et al., 2014) and the chemical composition of the pollution (Yi and Prybutok, 1996; Cincinelli et al., 2003; Querol et al., 2006; Minguillon et al., 2007; Huang et al., 2013) have been investigated. However, most of the studies focused on the analysis of field–monitored data. Further investigation with modeling applications is called for better understanding the importance of local emissions in the air pollution over industrialized areas (Figueiredo et al., 2013).

Previous air quality simulation works have shown that industry–intensive areas are weak points for air quality simulation. Wang et al. (2011) developed an integrated emission inventory for China and verified the CMAQ simulation results with observed data. The results suggested an overestimation for SO_2 and underestimation for PM_{10} in some industry–intensive areas because of the inaccurate allocation of emissions. An et al. (2013) verified the INTEX–2006 emission inventory using observation data from regional atmospheric background stations and found that the regional inventory failed to capture the influencing factors of strong regional sources on stations in China.

To improve the model performance, high–resolution modeling systems have been applied in some studies (Jang et al., 1995a; Jang et al., 1995b; Aguilera et al., 2013; Ferreira et al., 2013; Guttikunda and Calori, 2013). The use of a finer resolution provided some improvements in the simulations but did not always lead to better performance (Queen and Zhang, 2008; Liu and Zhang, 2013). Nishikawa and Kannari (2011) compared the emission maps within Osaka prefecture with both 1×1–km and 3×3–km mesh observations. NH_3 was found to be better represented at finer resolution, while NO_X showed the opposite results. The representation of SO_2 did not differ greatly between the two meshes. Valari and Menut (2008) noted that one of the principal sources of uncertainty affecting the model results for ozone (O_3) as the resolution increases is the input emission flux. Increased emission resolution was found to improve model results only up to a certain point, beyond which the induced noise became large. Fountoukis et al. (2013) examined the impact of grid resolution using the regional three–dimensional chemical transport model (CTM) PMCAMx (Particulate Matter Comprehensive Air quality Model with extensions) and found that the use of high resolution decreased the bias for BC (black carbon) and OA (organic aerosol) concentrations. Future work is suggested to combine high grid resolution with high–resolution emissions inventory. Shrestha et al. (2009) and Liu et al. (2010) also reported better performance using fine resolution and suggested applying the high–resolution models in studying highly urbanized regions with complex terrain and land–use as well as highly polluted areas. Because it remains unclear whether increasing resolution will positively influence the

model, there is a need for investigation on a local scale, especially in highly industrialized areas.

Baoshan District, one of the most important industrialized areas in China and the host of the most competitive steel and iron production plant in the world, was selected as the study area. The industrial sector, which is 60.1% of the size of the tertiary sector in 2009, dominates the regional economy and contributes extensively to local air pollution. A field study showed that industrial metallurgical processing and re–suspended soil dust are the major contributors of $PM_{0.43–2.1}$ and $PM_{2.1–10}$ in this district (Hu et al., 2014). Baoshan District is also suffering from rapid urbanization. The agricultural population decreased by 4.0% from 2005 to 2009 (BBS, 2009; SBS, 2009). In this work, the impact of spatial resolution on air quality simulation in this highly industrialized area was assessed. The WRF/CMAQ modeling system was operated at both 3–km and 1–km resolutions for January, April, July and October of 2009. In the first part of this study, we compare the allocation of emission inventory at 3–km and 1–km resolutions. In the second part, the WRF/CMAQ model performances at the two resolutions are temporally and spatially evaluated through ground level observations. Analysis of a specific site is conducted to further study the impact of resolution on air quality simulation in three typical area types (urban, industrial and rural).

2. Methodology

2.1. Overview of the study area

Baoshan District is located in the northeastern part of the Shanghai metropolitan area, at the junction of the Yangtze River and Huangpu River. It covers 280 km^2 (4.6% of Shanghai) and has a population of 1.4 million (7.1% of Shanghai). The regional Gross Domestic Product (GDP) increased by 12.1% to 91.3 billion Chinese Yuan in 2009, accounting for 6.1% of Shanghai's total GDP.

Steel and iron manufacturing and energy production are the major industries in the region. Baosteel Group Corporation is one of the most competitive steel and iron groups in the world, featuring the highest level of modernization of any group. It ranks second among the world's steel and iron enterprises (BAOSTEEL, 2012). Baosteel Group Corporation has four steel and iron manufacturing plants in Baoshan District, located in the towns of Luojing, Yuepu, Yanghang and Wusong (1, 2, 3 and 4, respectively, in Figure 1b). The town of Yuepu hosts one of the most productive power plants in Shanghai, the Huaneng Power plant (5 in Figure 1b), one of the largest listed power producers in China (HPI, 2011).

2.2. Local emission survey using the bottom–up method

To obtain a clear picture of the emission features of Baoshan District, a refined emission inventory at 1 km×1 km resolution has been developed using a completely bottom–up approach. There are 6 high–stack point sources and 623 medium to small–size point industrial sources in Baoshan District. The heights of the stacks and outlets emitting exhaust gas range from 20 m to 250 m based on the survey data (Tan et al., 2014). According to the survey of local industrial activities, industrial sources account for over 80% of all emissions of SO_2, NO_X and CO, of which approximately 70% come from the four Baosteel Plants and the Huaneng Power Plant. Transport sources (including road dust emission) are the main contributors of PM_{10} (85%) and $PM_{2.5}$ (70%). Specific emission characteristics were found in this highly industrialized area. The transport emissions of PM_{10} and $PM_{2.5}$ are much higher in Baoshan than in the Yangtze River Delta (YRD) region (Dong et al., 2009; Huang et al., 2011a). Heavy–duty trucks carrying material through the area have aggravated the emission conditions. Meanwhile, industrial emission of NH_3 is also much higher in Baoshan than in the YRD region, which has not been considered in most previous regional emission inventories (Tan et al., 2014). Field sampling analysis also showed that the source apportionment of particulate matter in this industrialized area is very different from that in the Putuo District, a residential/commercial area in Shanghai (Hu et al., 2014).

A local emission survey was conducted to develop a refined emission inventory to fulfill the requirements for a detailed study of the district. To improve the accuracy of both the emission amounts and the location of the emission sources, we updated the emission inventory based on the emission inventory developed by the Shanghai Environmental Monitoring Center (SEMC) (described in section 2.3). Special attention was paid to the two major industries, especially the location of outlets and the emission amounts of the four Baosteel plants, which account for approximately 90% of the regional industrial pollution. Field measurements using GPS instruments were conducted to determine the geographic positions of the major emission outlets scattered throughout the large plants. Based on the results, 99 major outlets are treated as isolated emission sources, and the emissions from other outlets were combined into these sources according to the principle of <Integrated Emission Standard of Air Pollutants (GB 16297–1996)> (MEP, 1996). Although the total emission amounts of the four plants can be derived from the China Pollution Source Censuses of 2007 and 2009, there are no separate emission data for each major outlet (CPSC, 2009). Here, two other databases developed for key pollution sources –the Charge Declaration of Key Pollution Sources and the Retrospective Environmental Impact Assessment Report– were used to obtain separate data for each major outlet. The former database provides detailed information for major discharge outlets, such as outlet height, yearly emission, exhaust control efficiency and monitored emission data. The latter database provides the emission amounts of important production processes as calculated by the methods of material balance. In this way, the accuracy of both the emission quantity and the locations of major industrial sources are guaranteed, and the data are more appropriate for further study in the highly industrialized district on local dimensions. Detailed information on the establishment of this emission inventory has been reported in the work of Tan et al. (2014).

We used ArcGIS tools to allocate the emission inventory. For the temporal allocation of emissions, we used profiles for different emission sources. In this study, these temporal variations were derived from local investigation. For the spatial allocation of emissions, we used GIS to distribute the emission sources. Stack emission sources, such as power plants and industrial sources, were distributed into grid cells according to their geographical position as determined by GPS instruments. Residential and agricultural sources were treated as area sources. We calculated the emissions of area sources at the town scale and used GIS tools to allocate emissions into grid cells. Transport sources were distributed according to the density of traffic flow.

2.3. Modeling system and setup

The WRF/CMAQ air quality modeling system was applied in this study. The next–generation mesoscale Advanced Research and Forecasting model (WRF–ARW, version 3.3) (Skamarock et al., 2008) was used to produce meteorological fields in three nested domains, as described in Figure 1a. Domain 1, a 252×207 cell grid, in size and was developed on a 9–km resolution covering Eastern China. Domain 2, covers all of Shanghai with a 84×75 cell grid at a 3–km spatial resolution. Domain 3, covers Baoshan District and was established on a 1–km spatial resolution with a 66×63 cell grid. The National Centers for Environmental Prediction (NECP) Final Analysis (FNL) data with a 1×1 resolution were used to provide the initial and boundary conditions for the WRF simulation with 24 sigma layers used for vertical resolution (NCEP, 2014). For the physical configuration, we used the WRF single–moment 6–class microphysics scheme, rapid radiative transfer model (RRTM) longwave radiation scheme, Dudhia shortwave radiation scheme, 5–layer thermal diffusion land surface scheme, MRF planetary

boundary layer scheme and Kain–Fritsch cumulus parameterization scheme. The WRF output files were processed by the Meteorology–Chemistry Interface Processor (MCIP) to create input meteorology files for CMAQ (Otte and Pleim, 2009).

A three–dimensional Eulerian atmospheric chemistry and transport model, CMAQ model version 4.6, was applied to simulate the concentrations of the major pollutants. Designed as a "one–atmosphere" model, CMAQ can address the complex couplings among several air quality issues simultaneously across spatial scales ranging from local to hemispheric (Byun and Ching, 1999; Byun and Schere, 2006). The model was run on domain 1 and domain 2 in January, April, July and October of 2010 as seasonal representatives. The boundary conditions were provided by the outputs from coarser grids. The vertical resolution includes 24 layers, with denser layers at lower altitudes. The corresponding layer heights were 19, 49, 99, 149, 249, 349, 500, 700, 900, 1 151, 1 316, 1 399, 1 569, 2 093, 2 274, 2 460, 2 942, 3 452, 4 565, 5 825, 7 308, 9 114, 11 456 and 14 294 m. We set 19 m as the height of the first layer because all the outlets in this study are above 20 m. In addition, 249 was set as the height for the fifth layer, as all outlets except the major outlets in the Baosteel Plants and Huaneng Power Plants are below that height. In this way, we can obtain a clear picture of the different types of emission outlets.

We used the CB5 scheme as the gas–phase chemical mechanism, Aero4 as the aerosol mechanism and Cloud_acm_ae5 as the liquid–phase chemical mechanism. The input emission inventory was unified from three differently established emission databases. For the areas inside Baoshan District, the local emission inventory described in Section 2.2 was applied. For the areas inside Shanghai but outside Baoshan, we used the emission inventory developed by the SEMC. This inventory was developed for major anthropogenic air pollutants and VOC species in Shanghai for the year 2009 at a 1 km×1 km resolution, considering industrial, transportation, residential and agricultural sources. For industrial sources, information such as geographical data, fuel consumption and the exhaust control efficiency of most industrial sources were collected using the database from the China Pollution Source Census (CPSC, 2009). The emission amounts were estimated by emission factor methods. The transport emissions were calculated by the International Vehicle Emission Model (IVE model), which is designed to estimate emissions from motor vehicles (ISSRC, 2014). The evaluation of the IVE model with remote sensing data revealed that it provides reasonable performance for the prediction of road carbon monoxide (CO) emissions but generally overestimates NO_X (Guo et al., 2007). Using a bottom–up approach, the emission inventory gives detailed information for major sources and provides higher accuracy than national– or continental–scale inventories. The general methods for developing the emission inventory have been applied in the development of emission inventories in the Pearl River Delta (PRD) and Yangtze River Delta (YRD) (Li et al., 2008; Zheng et al., 2009; Wang et al., 2010; Huang et al., 2011a; Huang et al., 2011b; Li et al., 2011).

For the areas outside Shanghai, Regional Emission Inventory in Asia and TRACE–P (Transport and Chemical Evolution over the Pacific) emission inventories were used. The REAS (Regional Emission Inventory in Asia) is the first emission inventory developed for Asia with the integration of the historical, present and future emissions of Asia based on a consistent methodology (Ohara et al., 2007). The most recent version provides SO_2, NO_X, CO, NMVOC, black carbon and organic carbon emissions from fuel combustion and industrial sources for the year 2009 with a resolution of 0.5×0.5. TRACE–P is an inventory of air pollutant emissions in Asia developed to support atmospheric modeling and the analysis of observations made during the TRACE–P experiment (Streets et al., 2003). It provides the emission data for SO_2, NO_X, CO_2, CO, CH_4, NMVOC, BC, OC and NH_3 at a 10×10 resolution. Comparing the two emission inventories, we adopted the CO, VOC_S and NH_3 emissions from REAS and the SO_2, NO_X, PM_{10} and $PM_{2.5}$ emissions from TRACE–P. Because there is no classification for emission sources in REAS, we applied the method used in TRACE–P and divided the pollution sources into power plants, other industrial sources and area sources. The unified inventory can provide general information for regional air pollution, but it has significant shortcomings. The mobile sources are categorized as area sources and cannot be treated separately. There is also an absence of heights for emission sources. The deficiencies have also been identified by modeling evaluation studies (Tan et al., 2004; Streets et al., 2006). Evaluating the TRACE–P emission inventory, Carmichael et al. (2003) reported major discrepancies between the modeled and observed pollutants in the Yellow Sea, with the model systematically underestimating the observations, and suggested an underestimation of the emissions from the domestic sector. Ma et al. (2006) compared the TRACE–P simulation results in China with the Global O_3 Monitoring Experiment (GOME) satellite data. The TRACE–P is found to underestimate the tropospheric nitrogen dioxide (NO_2) column density in all regions by more than 50% with respect to the GOME measurements. Thus, the use of these regional emission inventories may introduce high levels of uncertainty.

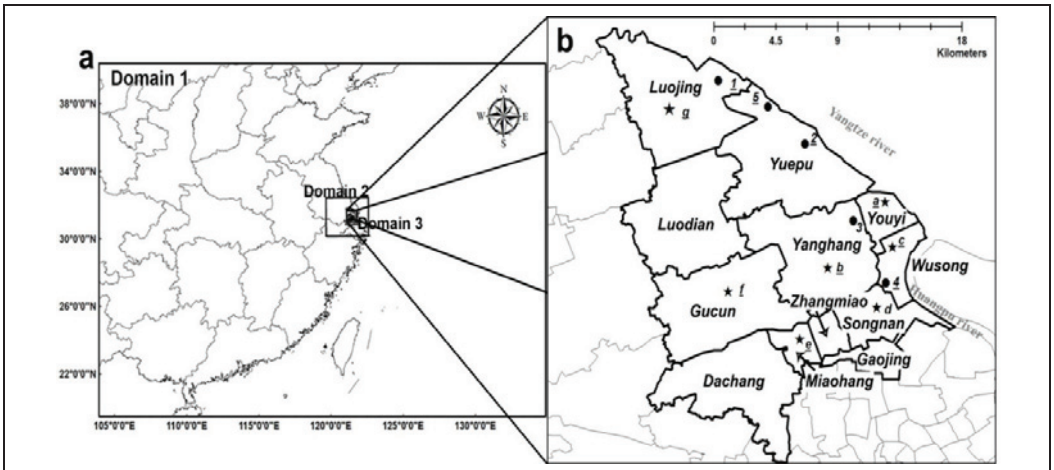

Figure 1. *Two model domains for CMAQ simulation* ***(a)*** *and the study area* ***(b).*** *Circle symbols represent the 5 major industrial emission sources: 1 Baosteel Heavy Plate Subsidiary, 2 Baosteel Plant, 3 Baosteel Special Steel Subsidiary, 4 Baosteel Stainless Steel Subsidiary, 5 Huaneng Power Plant. Star symbols represent the seven monitor stations: a Baoshan Monitor Center, b Yanghang Station, c Gangyansuo Station, d Songnan Station, e Miaohang Station, f Gucun Station, g Luojing Station.*

2.4. Observational data and evaluation methods

We used the hourly average observation data for air pollutants from 7 stations in the governmental standard monitoring network run by Baoshan Environmental Protection Bureau. The locations of 7 stations are presented in Figure 1b. Baoshan Monitoring Center is located in the town of Youyi in the city center. Gangyansuo and Songnan Stations are located in the towns of Wusong and Songnan, respectively, near the Baosteel Stainless Steel Subsidiary. These two stations are right in the regional industrial area. Yanghang and Gucun Stations are located in the towns of Yanghang and Gucun, respectively, relatively far from the heavy–industry plants. Luojing Station is located in the town of Luojing, where agriculture is still the main activity. Generally, these stations have a good representation of the concentrations at the regional level for different functional regions like urban, suburban and industrial.

The observational meteorological data from Baoshan Monitoring Center Station is used to assess WRF performance. The observation data are collected at 6–h intervals each day. The WRF results at two resolutions are verified in Section 3.2, and the CMAQ results are evaluated on a temporal scale in Section 3.3 and on a spatial scale in Section 3.4.

The model performance is evaluated by statistical indexes, including the relative error (RE), correlation coefficient (R), normalized mean bias (NMB), normalized mean error (NME) and root mean square error (RMSE). RE and NMB are measures of model bias, and NME and RMSE are measures of model error (Eder and Yu, 2006). The indexes are defined as:

$$\mathrm{RE} = \frac{S_i - O_i}{O_i} \times 100\% \tag{1}$$

$$\mathrm{R} = \frac{\sum_{i=1}^{n} S_i\, O_i}{\sqrt{(\sum_{i=1}^{n}|S_i|^2)(\sum_{i=1}^{n}|O_i|^2)}} = \frac{\sum_{i=1}^{n}(S_i - \bar{S_i})(O_i - \bar{O_i})}{\sqrt{\sum_{i=1}^{n}(S_i - \bar{S_i})^2 \sum_{i=1}^{n}(O_i - \bar{O_i})^2}} \tag{2}$$

$$NMB = \frac{\sum_{i=1}^{n}(S_i - O_i)}{\sum_{i=1}^{n} O_i} \times 100\% \tag{3}$$

$$NME = \frac{\sum_{i=1}^{n}|S_i - O_i|}{\sum_{i=1}^{n} O_i} \times 100\% \tag{4}$$

$$\mathrm{RMSE} = \sqrt{\frac{\sum_{i=1}^{n}(S_i - O_i)^2}{n}} \tag{5}$$

where, S_i is the simulation result, $\bar{S_i}$ is the mean of simulation results, O_i is the observation data, $\bar{O_i}$ is the mean of observation data.

3. Results and Discussion

3.1. Emission inventory allocation in 3–km– and 1–km–resolution grids

Highly industrialized areas are found to have specific emission features (Tan et al., 2014). Increasing the model resolution enhances the model's ability to represent emissions at the scale of individual cities (Chen et al., 2009). According to the emission inventory, industrial sources, especially the four Baosteel Plants and Huaneng Power Plant, are the main contributors to SO_2, NO_X and CO emissions. In the 1–km–resolution map (Figure 2), the towns of Yuepu and Wusong, the locations of the Baosteel Plants and Huaneng Power Plants, are characterized by high emissions. The PM_{10} emissions are spread throughout the district according to the traffic lines. The southeastern areas feature higher emission densities than the northwestern ones because of greater flow of vehicles in urban areas relative to rural areas. The industrial areas also have high emission densities due to the heavy–duty trucks carrying material through the area.

The emission features of this industrialized area are clearly presented using the fine–resolution grids. These emission features are also observed when using the coarse grid, but the coarser grids generally average the high emissions with nearby areas, yielding an unexpectedly high emission density for the neighboring areas and impairing the differentiation of various regions. This problem is significant for heavily polluted areas, such as the town of Yuepu and Wusong town. The finer–resolution network reveals the emission features of the highly industrialized area in more detail and provides more accurate input data for model simulation.

3.2. Evaluation of meteorological simulation

Metrology fields have a strong influence on the transport, diffusion, interaction and deposition processes of pollutants. The WRF simulation results at 3–km and 1–km resolutions were evaluated by comparison with the ground observations at the Baoshan Monitoring Center (Figure 3).

The temperature is well simulated by the WRF model at both resolutions. The modeled values are close to the observations except for an overestimation in January of 0.6° and 0.5° for the 3–km and 1–km resolutions, respectively. The model performs best in January (R=0.98 for both resolutions) and worst in July (R=0.83 for both). The relative humidity is underestimated in January (–5% for both) and April (–7% for 1 km and –12% for 3 km) but overestimated in July (7% for both) and December (2% for both). The model results at both resolutions are generally in good accordance with each other, except for the large difference from 4/18 to 4/21, when the model slightly underpredicts the temperature and missed the concentration peak of relative humidity at coarse resolution. The discrepancies between the two resolutions are not significant.

Wind speed is generally overestimated by the model at both resolutions, especially in July (over 26%) and December (over 30%). The model also fails to capture the peak timings in July at both resolutions (R=0.44 for 1 km and R=0.47 for 3 km) and largely overestimates the wind speed in December, especially after December 20th. Although the changing tendencies of the model results are well simulated, the model values are generally higher than the observations by 2 m/s, especially at fine resolution. It is also found that the model tends to give higher values at the end of each month. Wind direction is also modeled worst in July. However, the changing tendencies are generally well captured at both resolutions. We find some significant differences between the two resolutions on April 12th, April 22nd and July 4th, when the model results failed to match the observations at fine resolution, whereas the results at coarse resolution provide a better fit. In short, the model gives reasonable descriptions of wind speed at both resolutions, and the wind direction is slightly better modeled at coarse resolution.

3.3. Evaluation of temporal air quality trends at 3–km and 1–km resolutions

Figure 4 compares the simulation results at 3–km and 1–km resolutions with observations from Baoshan Monitoring Center. The SO_2 and NO emissions are highest in January and lowest in December, with significant seasonal variation, while the NO_2, CO and PM_{10} emissions are more stable throughout the year. This

result is in accord with that of Liu et al. (2010). The model succeeds in capturing the seasonal changing tendency of SO_2, NO, CO and PM_{10} at fine resolution, while missing some NO_2 peaks in the beginning of July. The coarser grid produces some unexpected concentration peaks for NO, NO_2 and PM_{10}, most evidently in December, and intensive peaks throughout the month, while the fine–resolution and observation values are rather stable. The difference is even greater in the CO simulation results.

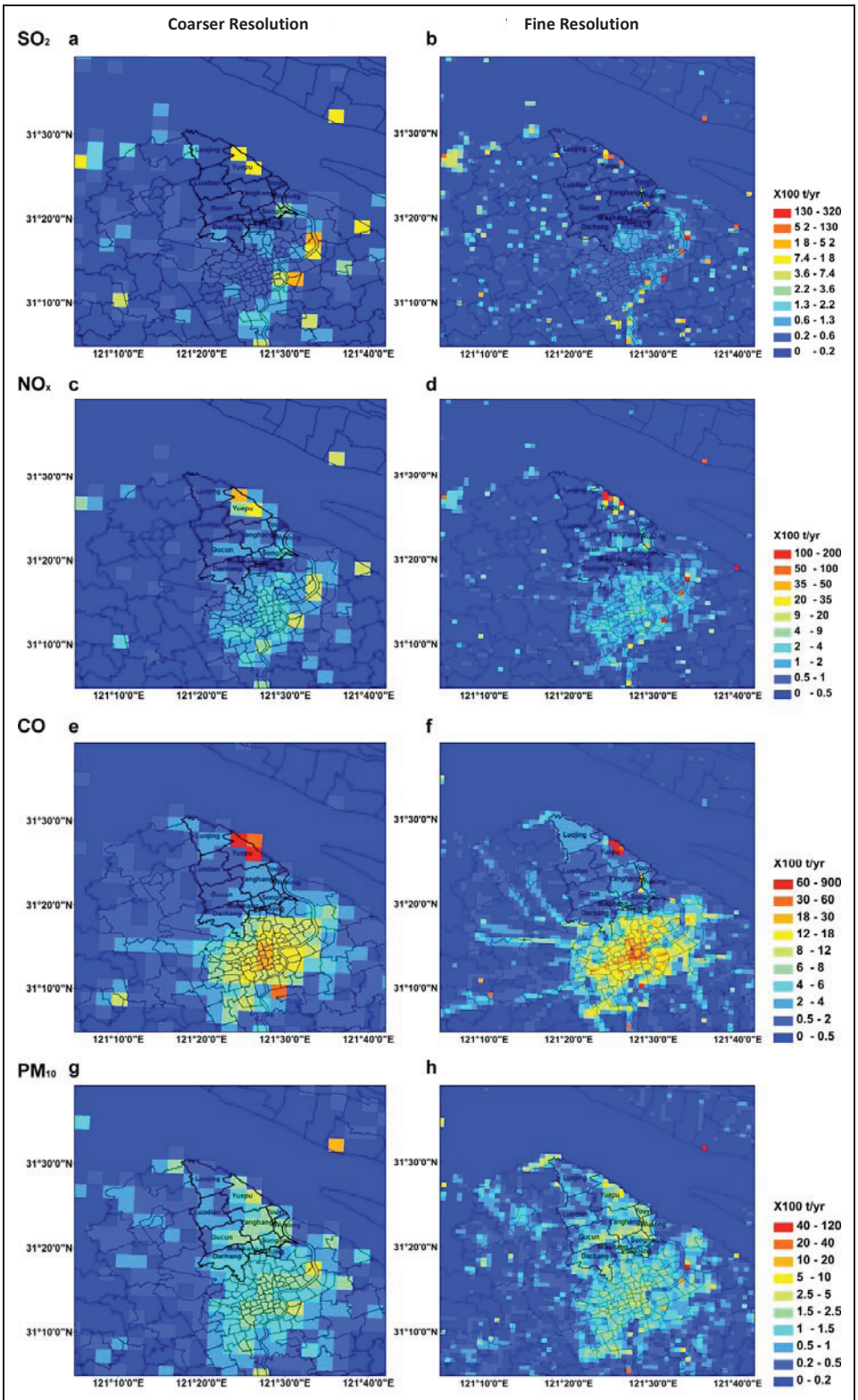

Figure 2. *Emission inventory of major pollutants in domain 2 at 3 km (left) and 1 km (right) resolutions.*

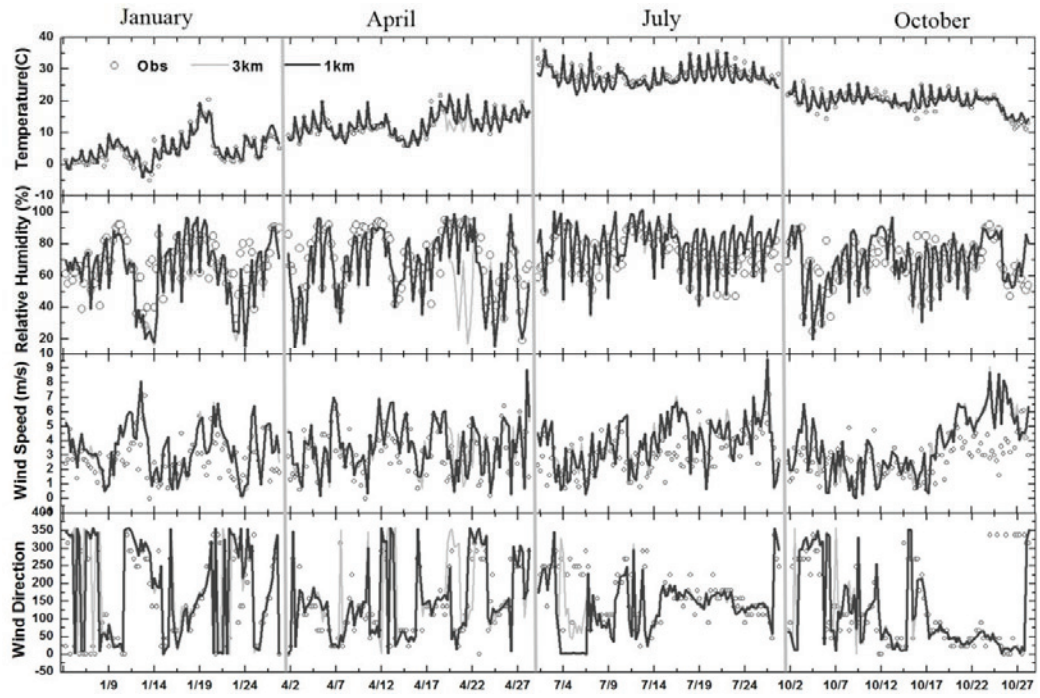

Figure 3. *WRF simulation results (6–hour interval) at Baoshan Monitor Center at 3 km resolution (light gray line) and 1 km resolution (dark gray line) are compared with ground observations (black circles).*

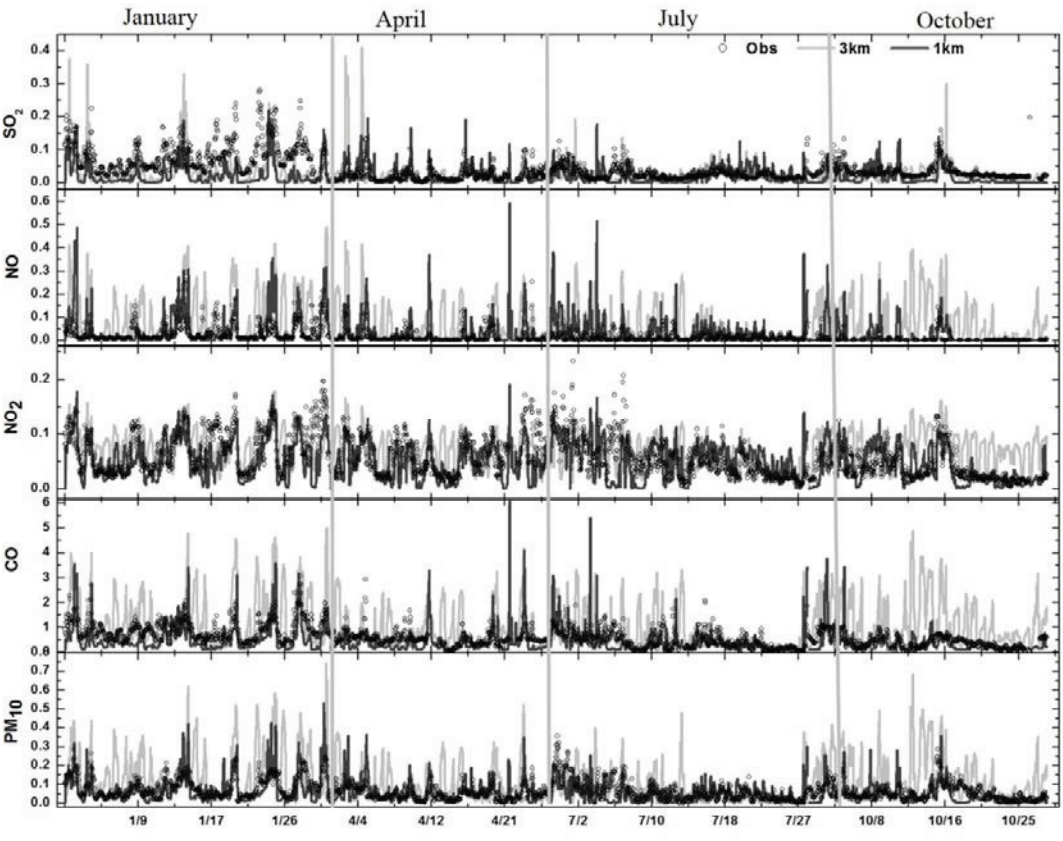

Figure 4. *CMAQ results [hourly concentration (mg/m^3)] at the Baoshan Monitor Center at 3 km resolution (light gray line) and 1 km resolution (dark gray line) are compared with ground observations (black circles).*

The model performs both best and worst in July. The model results are in good accordance with the observations for all the pollutants from July 13th to 26th, while all the pollutants except NO_2 are largely underpredicted and NO_2 is overestimated from July 1st to 6th. We noticed that the two episodes have opposite pollution trends. During the well–simulated episode, the concentrations of all the pollutants are the lowest among the four months, and the temporal variations are comparatively stable. In contrast, during the poorly simulated episode, the concentrations are rather high and constantly changing. The model tends to perform better in light pollution episodes than heavy pollution episodes. This may be because the model is less sensitive to the input of environmental parameters when simulating an episode at low pollution levels and thus partly eliminates the uncertainty caused by the meteorological field.

Table 1 summarizes the statistics for the hourly average model results at the 3–km and 1–km resolutions. SO_2 is underestimated by the model at coarse and fine resolutions (by 41% and 50%, respectively). For the other pollutants, the relative errors are lower for the fine resolution than the coarse resolution. The model overestimates the values by 26% to 245% at the 3–km resolution and –25% to 59% at the 1–km resolution. The NMB, NME and RMSE also illustrate that use of fine resolution brings the model results closer to the observations. The temporal variations of NO_2, CO and PM_{10} are also better captured by the finer resolution, with a correlation coefficient of approximately 0.3 (weakly related) at 3 km to over 0.5 (moderately related) at 1 km.

It should be noted that SO_2 is the only pollutant modeled worse at finer resolution. Although the model yields higher values in January than in the other three months, it still underestimates the concentrations by 70%. The same result was also reported in the work of An et al. (2013) when simulating the INTEX–B2006 emission inventory. The SO_2 of Linan (a station representing the Yangtze River Delta) was found to be underestimated to a larger extent in winter than in the other seasons, while the correlation between the observed and simulated data in winter (0.6) was better than that in summer and autumn (approximately 0.5 and 0.55, respectively). However, severe SO_2 pollution has been a major problem in Beijing during the heating period of winter (Huang et al., 2011a). In some studies, SO_2 is overestimated in winter, when vertical and horizontal transport is a major factor affecting SO_2 concentration because chemical oxidation is slow (Luo et al., 2011). The long–term transport from North China to the YRD also reinforces the pollution caused by large local emissions (Li et al., 2011). In this work, the long–term transport from North China is not completely considered because the simulating domain for CMAQ is not large enough to include all the North China regions. Meanwhile, the SO_2 emissions may be underestimated in the TRACE–P inventory because the INTEX–B inventory, as an update of the TRACE–P, has been found to underestimate SO_2 in winter in the YRD region (Zhang et al., 2009; An et al., 2013). Moreover, the CMAQ was found to poorly simulate the SO_2 daily variation characteristics because of the inadaptability of emission time–variant factors (Xie et al., 2012).

3.4. Evaluation of the spatial distribution of air quality at 3–km and 1–km resolutions and comparison of model performances in urban, rural and industrial areas

The spatial distributions of the major pollutants at resolutions of 3 km (left) and 1 km (right) are shown in Figure 5. Generally, the distributions in both maps exhibit good consistency with the emission allocation illustrated in Section 3.1. The maximum concentration in Baoshan District is located in the major industrial center and along the major traffic line in the local urban center. However, the finer–resolution map shows a clearer pollution diffusion tendency with much higher concentrations in polluted areas than in the nearby areas. In the coarser map, the spatial discrepancies are averaged and thus less distinct between industrial and non–industrial areas. Table 2 presents the relative error at both resolutions at the seven monitoring stations. The performance of the finer grid is obviously better than that of the coarser grid. The coarser–grid model generally overestimated the concentration of all pollutants except SO_2. High model errors are found in the sites near the high–concentration areas, such as Baoshan Monitoring Center near the industrial center and the town of Miaohang near the urban center, where NO is over-predicted by 278% and 401%, respectively. In the other areas, such as the town of Luojing, the differences between the two resolutions are less obvious. It is clear that finer grids give more accurate results for heavily polluted areas than coarser grids. In particular, the Gangyansuo station, as a site located in the industrial center, is simulated best (Table 2), indicating the important role of the finer emission inventory in industrial regions.

Further analysis was conducted on specific sites to study the model performance on different types of areas in this area. Gangyansuo station, located in the industrial center near the boundary between Wusong town and the town of Songnan, represents an industrial area; Baoshan Monitoring Center, located on Youyi Street, is a typical urban site; and Luojing station, located in the north of Baoshan, where agriculture is still common, is the representative of rural areas. Figure 6 summarizes the statistical evaluations of model performance at both resolutions. The model overestimates all pollutants except SO_2 at 3–km resolution in all the sites, and the performances are obviously improved at finer resolution. Large errors are found for the urban site, where both the NMB and NME indexes of NO reached 300. The daily averaged concentrations of major pollutants at 3–km (filled points) and 1–km (empty points) resolutions are presented in Figure 7. In the urban and rural sites, the fine–resolution results have much higher *R* values for all pollutants except SO_2. In the industrial site, the model performed badly at fine resolution, with *R* values much lower than those at coarse resolution. The model accuracies for SO_2, NO_X and PM_{10} in predicting exceeding air quality standards are presented in Table 2. Although the model did not improve predicting SO_2 using finer resolution, NO_X and PM_{10} exceeding conditions are better predicted. The accuracies at 3–km resolution differ from 57% to 90% and finer resolution improved the values to 71%–90%.

Table 1. *Statistical performance (hourly averaged) model at Baoshan Monitor Center at 3 km and 1 km resolutions*

Pollutants	Resolution	Relative Error (%)	Correlation (R)	NMB (%)	NME (%)	RMSE (μg/m³)
SO_2	3 km	–40.8	0.27	–39.15	70.82	0.05
	1 km	–49.7	0.35	–48.34	75.44	0.04
NO	3 km	245.0	0.33	291.34	344.75	0.10
	1 km	58.6	0.37	79.93	160.12	0.06
NO_2	3 km	25.8	0.26	28.32	65.02	0.05
	1 km	–11.9	0.50	–10.16	48.48	0.04
CO	3 km	74.8	0.35	83.34	120.06	1.01
	1 km	–24.9	0.51	–21.23	60.27	0.52
PM_{10}	3 km	74.4	0.36	76.15	119.01	0.12
	1 km	–12.7	0.51	–11.82	61.94	0.06

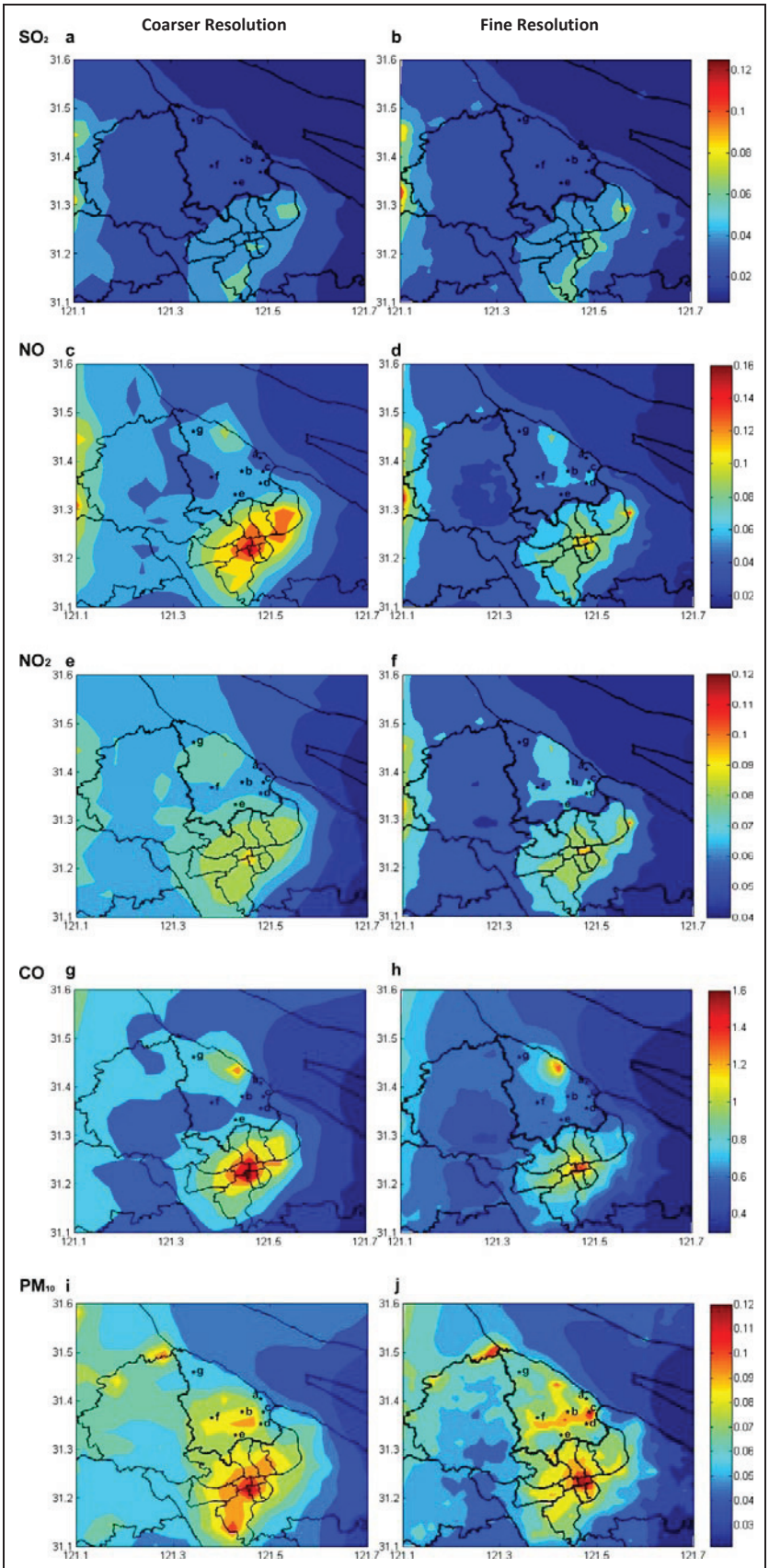

Figure 5. *Spatial distribution of major pollutants at 3 km (left) and 1 km (right) resolutions (mg/m^3). Star symbols represent the 7 monitoring stations.*

Table 2. *Relative error of model results at the seven monitor stations at 3 km and 1 km resolutions (%)*

Stations		(a) Baoshan Monitor Center	(b) Yanghang	(c) Gangyansuo	(d) Songnan	(e) Miaohang	(f) Gucun	(g) Luojing
SO_2	3 km	–39.3	–41.3	–36.1	–42.6	17.2	0.6	–47.7
	1 km	–48.7	–40.5	–32.5	–41.4	–4.4	–22.6	12.3
NO	3 km	277.8	63.3	39.6	145.3	401.1		30.4
	1 km	71.5	17.3	7.9	55.8	136.0		64.9
NO_2	3 km	27.2	14.4	4.7	–11.8	31.0	150.8	18.9
	1 km	–11.3	4.6	0.7	–17.2	8.1	100.1	33.6
CO	3 km	78.9		0.6		42.9	2.2	–5.6
	1 km	–23.8		–27.3		–42.2	–59.9	–22.4
PM_{10}	3 km	76.1	20.5	33.9	53.0	78.3	136.9	–11.0
	1 km	–12.8	–4.6	–2.7	–9.7	28.2	14.8	–5.8

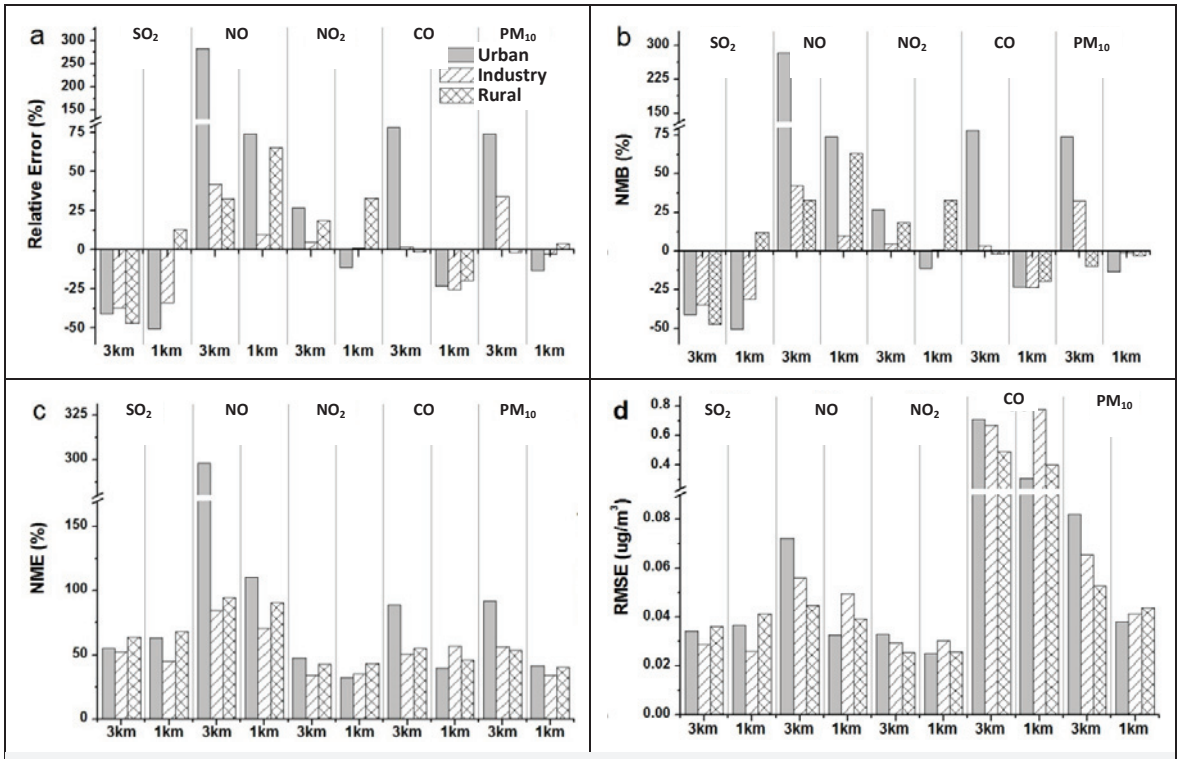

Figure 6. *Statistical performance (daily averaged) at 3 km and 1 km resolution in the urban site, industrial site, and rural site.*

Among the three area types, the urban area is better predicted at fine resolution in terms of both the magnitude and the variation tendency. In the rural area, the coarser grid did not deteriorate the model performance, and the results at the two resolutions are quite similar. The emission inventory in rural area is considered to be one of the main reasons for this. The contributions of emissions related to agricultural activities such as fertilization, animal husbandry and outdoor biomass burning are higher in rural areas than in industrial and urban areas. The emissions were calculated by the emission factor method using the activity data collected from statistical yearbooks, and the emission amounts are not as refined as in the industrial and urban areas, thus reducing the impact of model grid resolution. Meanwhile, the lack of studies on the daily variation factors of agriculture has also induced errors in simulating the changing tendency of pollution in rural areas. For the industrial site, although the emission amount is modeled better than that at any other site at fine resolution, the changing tendency is not captured well. On the contrary, coarse grids simulated the changing tendency well, with very high *R* values, but failed to capture the magnitude of the pollution level. We also noticed that the *R* values in the fine–resolution results for CO were for the urban (0.64) and rural (0.47) sites but low for the industrial site (<0.1). Because CO has simple removal mechanisms in the atmosphere, the model performance is strongly influenced by meteorological conditions, especially wind speed and wind direction. The temporal emission allocation is also considered as one the main reasons. The same temporal allocation profile was used for all industrial sources except power plants, and these discrepancies may increase the uncertainty in simulating the changing tendencies.

4. Conclusions

The impact of spatial resolution on air quality simulation in a typical industrial area was investigated in this study. The difference between the emission inventories allocated in 3–km– and 1–km–resolution grids illustrates that the emission inventory allocated at a finer resolution gives more detailed information over the industrial area. The model resolution has a minor impact on simulating meteorological factors but an important influence on air quality simulation.

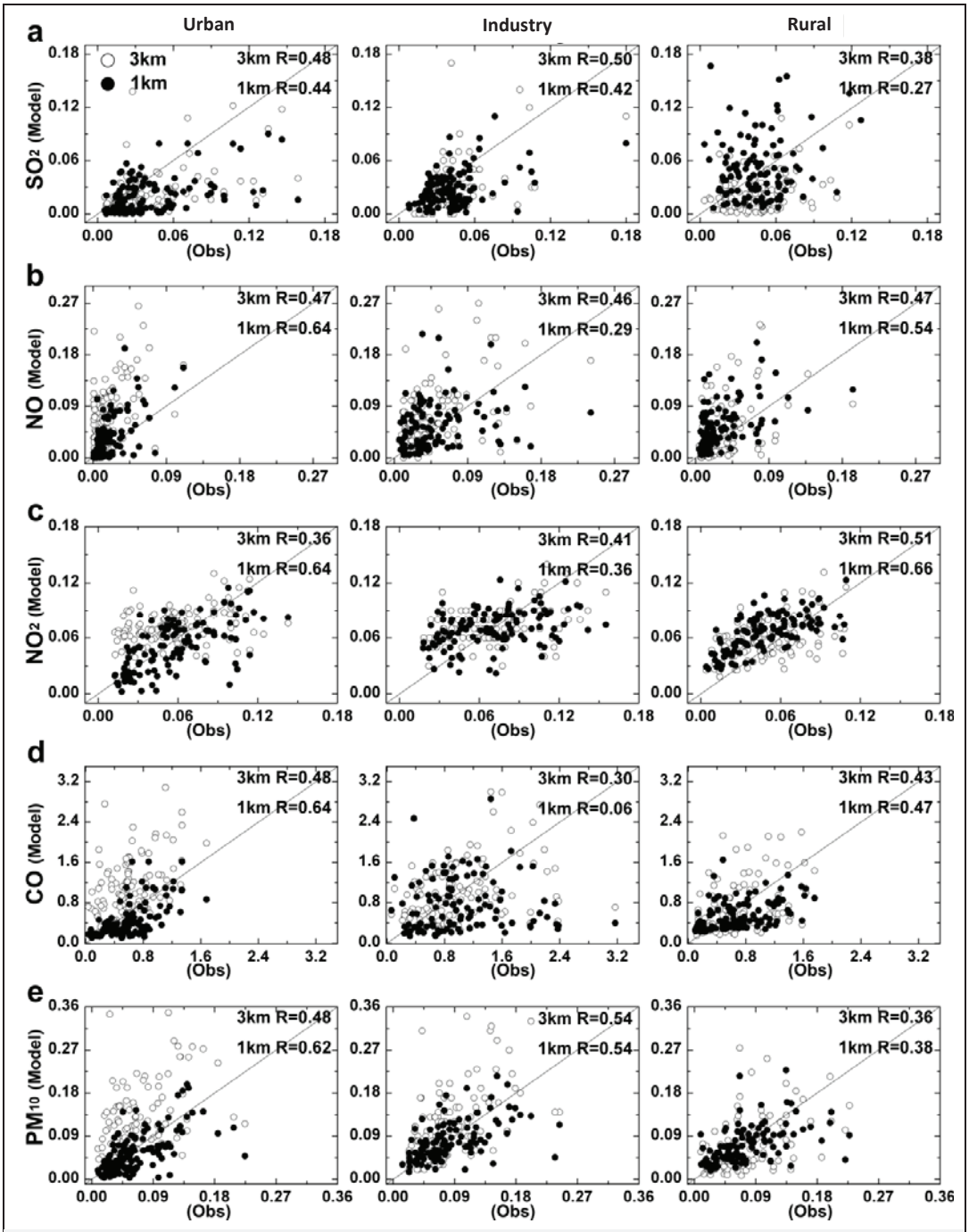

Figure 7. *CMAQ results (daily averaged (mg/m^3) at 3 km (empty point) and 1 km resolution (filled point) in the urban, industrial and rural sites.*

The CMAQ performances at the two resolutions were evaluated by ground observations both temporally and spatially. In the temporal evaluation, the model performance is improved by the use of the finer resolution in terms of capturing both the magnitudes and the variation for all the pollutants except SO_2. The relative errors range from 26% to 245% at coarse resolution but only –25% to 59% at fine resolution. The changing tendencies for NO_2, CO and PM_{10} are improved from approximately 0.3 at coarse resolution to over 0.5 at fine resolution. Many unexpected concentration peaks are produced at coarse resolution, especially in December. SO_2 is underestimated by both resolutions, especially in winter at fine resolution because the long–term transportation from North China during the heating season is underpredicted. In the spatial evaluation, the relative errors at the seven monitoring stations range from –43% to 401% at coarse resolution and –60% to 136% at fine resolution. Although the performance is not improved for all sites by increasing the model resolution, a fine–resolution network is more generally accurate for simulating industry–intensive areas. A coarser network generally overestimates all pollutants except SO_2, especially in sites near heavily polluted areas.

Further comparison of the three types of areas (urban, industrial and rural) showed that the urban area is better predicted at fine resolution in terms of both magnitude and variation tendency. In the rural area, the impact of resolution was not significant, possibly because of the emission inventory used. In the industrial area, although the coarse grid captured the changing tendency well, with very high R values, it failed to capture the magnitude of the pollution level. On the contrary, the fine grid succeeded in predicting the pollution level but failed for the temporal variation. Inadequate study of the temporal allocation for different industrial sources is very likely to increase the uncertainty. Meteorological conditions, especially wind speed and wind direction may also account for the simulation errors in this case.

A high–resolution modeling system coupled with a refined emission inventory was applied to simulate the air quality in a highly industrialized area. The accuracies of both the emission profile and the meteorological field were the key points. To improve the accuracy of the emission profile, collecting detailed information on local industrial activities is suggested. Regarding the meteorological simulation, the model deviation from the real meteorological conditions is only slightly reduced by the high–resolution network, and the result is still inadequate for representing the real conditions, especially in the areas with intensive emission sources. Further study focusing on the combined improvement of the local meteorological field and emission profile is needed to achieve better simulation results.

Acknowledgments

This work was supported by the National Natural Science Foundation of China (Grant No.41005076 and No.71173049) and Science and Technology Commission of Shanghai Municipality (Grant No. 14ZR1402800 and No. 12DJ1400100). This study is partly funded by the open fund from Jiangsu Key Laboratory of Atmospheric Environment Monitoring and Pollution Control and a project funded by the Priority Academic Program Development of Jiangsu Higher Education Institutions (PAPD).Special thanks to Shanghai Environmental Monitoring Center and Shanghai City Comprehensive Transportation Planning Institute for sharing their traffic emission data. Thanks to meteorological data from Baoshan Meteorology Bureau and air quality data from Baoshan Environmental Bureau.

References

Aguilera, I., Basagana, X., Pay, M.T., Agis, D., Bouso, L., Foraster, M., Rivera, M., Baldasano, J.M., Kunzli, N., 2013. Evaluation of the CALIOPE air quality forecasting system for epidemiological research: The example of NO_2 in the province of Girona (Spain). *Atmospheric Environment* 72, 134–141.

An, X.Q., Sun, Z.B., Lin, W.L., Jin, M., Li, N., 2013. Emission inventory evaluation using observations of regional atmospheric background stations of China. *Journal of Environmental Sciences–China* 25, 537–546.

BAOSTEEL, 2012. http://www.baosteel.com/group_en/contents/2880/39991.html, accessed on October 2014.

BBS (Baoshan Bureau of Statistics), 2009. Baoshan Statistical Yearbook, 2009. http://bstj.baoshan.sh.cn/tjsj/tjnj/201007/t20100719_33511.html, accessed in October 2014.

Byun, D., Schere, K.L., 2006. Review of the governing equations, computational algorithms, and other components of the models–3 Community Multiscale Air Quality (CMAQ) modeling system. *Applied Mechanics Reviews* 59, 51–77.

Byun, D., Ching, J., 1999. Science algorithms of the EPA models–3 Community Multiscale Air Quality (CMAQ) Modeling System, U.S. EPA (United States Environmental Protection Agency), Report No. EPA–600/R–99/030.

Carmichael, G.R., Tang, Y., Kurata, G., Uno, I., Streets, D.G., Thongboonchoo, N., Woo, J.H., Guttikunda, S., White, A., Wang, T., Blake, D.R., Atlas, E., Fried, A., Potter, B., Avery, M.A., Sachse, G.W., Sandholm, S.T., Kondo, Y., Talbot, R.W., Bandy, A., Thorton, D., Clarke, A.D., 2003. Evaluating regional emission estimates using the TRACE–P observations. *Journal of Geophysical Research–Atmospheres* 108, art. no. 8820.

Chan, C.K., Yao, X., 2008. Air pollution in mega cities in China. *Atmospheric Environment* 42, 1–42.

Chen, D., Wang, Y., McElroy, M.B., He, K., Yantosca, R.M., Le Sager, P., 2009. Regional CO pollution and export in China simulated by the high–resolution nested–grid GEOS–Chem model. *Atmospheric Chemistry and Physics* 9, 3825–3839.

Cincinelli, A., Mandorlo, S., Dickhut, R.M., Lepri, L., 2003. Particulate organic compounds in the atmosphere surrounding an industrialised area of Prato (Italy). *Atmospheric Environment* 37, 3125–3133.

CPSC (China Pollution Source Census), 2009. http://cpsc.mep.gov.cn, accessed in October 2014.

Dong, Y.Q., Chen, C.H., Huang, C., Wang, H.L., Li, L., Dai, P., Jia, J.H., 2009. Anthropogenic emissions and distribution of ammonia over the Yangtze River Delta. *Acta Scientiae Circumstantiae* 29, 1611–1617 (in Chinese).

Eder, B., Yu, S.C., 2006. A performance evaluation of the 2004 release of models–3 CMAQ. *Atmospheric Environment* 40, 4811–4824.

Ferreira, J., Guevara, M., Baldasano, J.M., Tchepel, O., Schaap, M., Miranda, A.I., Borrego, C., 2013. A comparative analysis of two highly spatially resolved European atmospheric emission inventories. *Atmospheric Environment* 75, 43–57.

Figueiredo, M.L., Monteiro, A., Lopes, M., Ferreira, J., Borrego, C., 2013. Air quality assessment of Estarreja, an urban industrialized area, in a coastal region of Portugal. *Environmental Monitoring and Assessment* 185, 5847–5860.

Fountoukis, C., Koraj, D., van der Gon, H.A.C.D., Charalampidis, P.E., Pilinis, C., Pandis, S.N., 2013. Impact of grid resolution on the predicted fine PM by a regional 3–D chemical transport model. *Atmospheric Environment* 68, 24–32.

Guo, H., Zhang, Q.Y., Shi, Y., Wang, D.H., 2007. Evaluation of the International Vehicle Emission (IVE) model with on–road remote sensing measurements. *Journal of Environmental Sciences–China* 19, 818–826.

Guttikunda, S.K., Calori, G., 2013. A GIS based emissions inventory at 1 km x 1 km spatial resolution for air pollution analysis in Delhi, India. *Atmospheric Environment* 67, 101–111.

HPI (Huaneng Power International, INC),2011. http://www.hpi.com.cn/sites/english/Pages/companyprofile.aspx, accessed on October 2014.

Hu, Z.M., Wang, J., Chen, Y.Y., Chen, Z.L., Xu, S.Y., 2014. Concentrations and source apportionment of particulate matter in different functional areas of Shanghai, China. *Atmospheric Pollution Research* 5, 138–144.

Huang, B., Liu, M., Ren, Z.F., Bi, X.H., Zhang, G.H., Sheng, G.Y., Fu, J.M., 2013. Chemical composition, diurnal variation and sources of $PM_{2.5}$ at two industrial sites of South China. *Atmospheric Pollution Research* 4, 298–305.

Huang, C., Chen, C.H., Li, L., Cheng, Z., Wang, H.L., Huang, H.Y., Streets, D.G., Wang, Y.J., Zhang, G.F., Chen, Y.R., 2011a. Emission inventory of anthropogenic air pollutants and VOC species in the Yangtze River Delta region, China. *Atmospheric Chemistry and Physics* 11, 4105–4120.

Huang, C., Chen, C.H., Li, L., Cheng, Z., Wang, H.L., Wang, Y.J., Huang, H.Y., Zhang, G.F., Chen, Y.R., 2011b. Anthropogenic air pollutant emission characteristics in the Yangtze River Delta region, China. *Acta Scientiae Circumstantiae* 31, 1858–1871 (in Chinese) .

ISSRC (International Sustainable System Research Center), 2014. International Vehicle Emission Model (IVE Model), http://www.issrc.org/ive/, accessed in October 2014.

Jang, J.C.C., Jeffries, H.E., Byun, D., Pleim, J.E., 1995a. Sensitivity of ozone to model grid resolution – I. Application of high–resolution regional acid deposition model. *Atmospheric Environment* 29, 3085–3100.

Jang, J.C.C., Jeffries, H.E., Tonnesen, S., 1995b. Sensitivity of ozone to model grid resolution – II. Detailed process analysis for ozone chemistry. *Atmospheric Environment* 29, 3101–3114.

Li, L., Chen, C.H., Fu, J.S., Huang, C., Streets, D.G., Huang, H.Y., Zhang, G.F., Wang, Y.J., Jang, C.J., Wang, H.L., Chen, Y.R., Fu, J.M., 2011. Air quality and emissions in the Yangtze River Delta, China. *Atmospheric Chemistry and Physics* 11, 1621–1639.

Li, L., Chen, C.C., Cheng, H., Huang, H.Y., Li, Z.P., Fu, J.S., Carey, J.J., Streets, D.G., 2008. Regional air pollution characteristics simulations of O_3 and PM_{10} over Yangtze River Delta region, *Environmental Science* 29, 237–245 (in Chinese).

Liu, X.H., Zhang, Y., 2013. Understanding of the formation mechanisms of ozone and particulate matter at a fine scale over the southeastern U.S.: Process analyses and responses to future–year emissions. *Atmospheric Environment* 74, 259–276.

Liu, X.H., Zhang, Y., Cheng, S.H., Xing, J., Zhang, Q.A., Streets, D.G., Jang, C., Wang, W.X., Hao, J.M., 2010. Understanding of regional air pollution over China using CMAQ, Part I performance evaluation and seasonal variation. *Atmospheric Environment* 44, 2415–2426.

Luo, C., Wang, Y.H., Mueller, S., Knipping, E., 2011. Diagnosis of an underestimation of summertime sulfate using the Community Multiscale Air Quality model. *Atmospheric Environment* 45, 5119–5130.

Ma, J., Richter, A., Burrows, J.P., Nuss, H., van Aardenne, J.A., 2006. Comparison of model–simulated tropospheric NO_2 over China with GOME–satellite data. *Atmospheric Environment* 40, 593–604.

MEP (Ministry of Environmental Protection of the People's Republic of China), 1996. *GB 16297–1996 Integrated Emission Standard of Air Pollutants*, http://kjs.mep.gov.cn/hjbhbz/bzwb/dqhjbh/dqgdwrywrwpfbz/199701/t19970101_67504.htm, accessed in October 2014.

Minguillon, M.C., Querol, X., Alastuey, A., Monfort, E., Mantilla, E., Sanz, M.J., Sanz, F., Roig, A., Renau, A., Felis, C., Miro, J.V., Artinano, B., 2007. PM_{10} speciation and determination of air quality target levels. A case study in a highly industrialized area of Spain. *Science of the Total Environment* 372, 382–396.

NCEP (National Center for Environmental Protection), 2014. http://rda.ucar.edu/datasets/ds083.2/, accessed in October 2014.

Nishikawa, Y., Kannari, A., 2011. Atmospheric concentration of ammonia, nitrogen dioxide, nitric acid, and sulfur dioxide by passive method within Osaka prefecture and their emission inventory. *Water, Air, and Soil Pollution* 215, 229–237.

Ohara, T., Akimoto, H., Kurokawa, J., Horii, N., Yamaji, K., Yan, X., Hayasaka, T., 2007. An Asian emission inventory of anthropogenic emission sources for the period 1980–2020. *Atmospheric Chemistry and Physics* 7, 4419–4444.

Otte, T.L., Pleim, J.E., 2009. The meteorology–chemistry interface processor (MCIP) for the CMAQ modeling system. *Geoscientific Model Development Discussions* 2, 1449–1486.

Queen, A., Zhang, Y., 2008. Examining the sensitivity of MM5–CMAQ predictions to explicit microphysics schemes and horizontal grid resolutions, Part III – The impact of horizontal grid resolution. *Atmospheric Environment* 42, 3869–3881.

Querol, X., Zhuang, X., Alastuey, A., Viana, M., Lv, W., Wang, Y., Lopez, A., Zhu, Z., Wei, H., Xu, S., 2006. Speciation and sources of atmospheric aerosols in a highly industrialised emerging mega–city in Central China. *Journal of Environmental Monitoring* 8, 1049–1059.

SBS (Shanghai Bureau of Statistics), 2009. *Shanghai Statistical Yearbook 2009*, Chinese National Press, Shanghai, China.

Shrestha, K.L., Kondo, A., Kaga, A., Inoue, Y., 2009. High–resolution modeling and evaluation of ozone air quality of Osaka using MM5–CMAQ system. *Journal of Environmental Sciences–China* 21, 782–789.

Skamarock, W.C., Klemp, J.B., Dudhia, J., Gill, D.O., Barker, D.M., Duda, M.G., Huang, X.Y., Wang, W., Powers, J.G., 2008. A description of the Advanced Research WRF Version 3, NCAR Technical Note TN–475+STR, http://www.mmm.ucar.edu/wrf/users/docs/arw_v3.pdf.

Streets, D.G., Zhang, Q., Wang, L.T., He, K.B., Hao, J.M., Wu, Y., Tang, Y.H., Carmichael, G.R., 2006. Revisiting China's CO emissions after the Transport and Chemical Evolution over the Pacific (TRACE–P) mission: Synthesis of inventories, atmospheric modeling, and observations. *Journal of Geophysical Research–Atmospheres* 111, art. no. D14306.

Streets, D.G., Bond, T.C., Carmichael, G.R., Fernandes, S.D., Fu, Q., He, D., Klimont, Z., Nelson, S.M., Tsai, N.Y., Wang, M.Q., Woo, J.H., Yarber, K.F., 2003. An inventory of gaseous and primary aerosol emissions in Asia in the year 2000. *Journal of Geophysical Research–Atmospheres* 108, art. no. 8809.

Tan, J.N., Yu, Q., Ma, W.C., Ma, J.L., Cheng, J., Zhang, Y., 2014. Development of refined emission inventory of air pollutants: A case study of Shanghai Baoshan District. *Acta Scientiae Circumstantiae* 34, 1099–1108 (in Chinese).

Tan, Q., Chameides, W.L., Streets, D., Wang, T., Xu, J., Bergin, M., Woo, J., 2004. An evaluation of TRACE–P emission inventories from China using a regional model and chemical measurements. *Journal of Geophysical Research–Atmospheres* 109, art. no. D22305.

Tsai, Y.I., Kuo, S.C., Lee, W.J., Chen, C.L., Chen, P.T., 2007. Long–term visibility trends in one highly urbanized, one highly industrialized, and two rural areas of Taiwan. *Science of the Total Environment* 382, 324–341.

Valari, M., Menut, L., 2008. Does an increase in air quality models' resolution bring surface ozone concentrations closer to reality? *Journal of Atmospheric and Oceanic Technology* 25, 1955–1968.

Wang, S.X., Xing, J., Chatani, S., Hao, J.M., Klimont, Z., Cofala, J., Amann, M., 2011. Verification of anthropogenic emissions of China by satellite and ground observations. *Atmospheric Environment* 45, 6347–6358.

Wang, X., Zhang, Y., Hu, Y., Zhou, W., Lu, K., Zhong, L., Zeng, L., Shao, M., Hu, M., Russell, A.G., 2010. Process analysis and sensitivity study of regional ozone formation over the Pearl River Delta, China, during the PRIDE–PRD2004 campaign using the Community Multiscale Air Quality modeling system. *Atmospheric Chemistry and Physics* 10, 4423–4437.

Xie, M., Zhong, L.J., Chen, H.S., Chen, D.H., 2012. Application and verification of CMAQ model and revision forecast in Pearl River Delta region. *Environmental Science & Technology* 35, 96–101 (in Chinese).

Yi, J.S., Prybutok, V.R., 1996. A neural network model forecasting for prediction of daily maximum ozone concentration in an industrialized urban area. *Environmental Pollution* 92, 349–357.

Zhang, Q., Streets, D.G., Carmichael, G.R., He, K.B., Huo, H., Kannari, A., Klimont, Z., Park, I.S., Reddy, S., Fu, J.S., Chen, D., Duan, L., Lei, Y., Wang, L.T., Yao, Z.L., 2009. Asian emissions in 2006 for the NASA INTEX–B mission. *Atmospheric Chemistry and Physics* 9, 5131–5153.

Zheng, J.Y., Zhang, L.J., Che, W.W., Zheng, Z.Y., Yin, S.S., 2009. A highly resolved temporal and spatial air pollutant emission inventory for the Pearl River Delta region, China and its uncertainty assessment. *Atmospheric Environment* 43, 5112–5122.